AD-A232 124

DTIC FILE COPY

GL-TR-90-0224
ENVIRONMENTAL RESEARCH PAPERS, NO. 1072

LABORATORY STUDY OF THE THERMOCHEMICAL PROPERTIES OF MATERIALS USED IN SPACECRAFT

TERRY L. THIEM, 1LT, USAF
LYN R. WATSON
RAINER A. DRESSLER
RICHARD H. SALTER
EDMOND MURAD

DTIC
ELECTE
MAR 0 5 1991
S B D

4 SEPTEMBER 1990

Approved for public release; distribution unlimited.

SPACE PHYSICS DIVISION PROJECT 7601
GEOPHYSICS LABORATORY
HANSCOM AFB, MA 01731-5000

91 3 01 031

"This technical report has been reviewed and is approved for publication"

E. Murad

for CHARLES P. PIKE, Chief
Spacecraft Interactions Branch

FOR THE COMMANDER

WILLIAM SWIDER, Deputy Director
Space Physics Division

This report has been reviewed by the ESD Public Affairs Office (PA) and is releasable to the National Technical Information Service (NTIS)

Qualified requestors may obtain additional copies from the Defense Technical Information Center. All others should apply to the National Technical Information Service.

If your address has changed, or if you wish to be removed from the mailing list, or if the addressee is no longer employed by your organization, please notify AFGL/DAA, Hanscom AFB, MA, 01731. This will assist us in maintaining a current mailing list.

Do not return copies of this report unless contractual obligations or notices on a specific document requires that it be returned.

REPORT DOCUMENTATION PAGE

Form Approved
OMB No. 0704-0188

Public reporting burden for this collection of information is estimated to average 1 hour per response, including the time for reviewing instructions, searching existing data sources, gathering and maintaining the data needed, and completing and reviewing the collection of information. Send comments regarding this burden estimate or any other aspect of this collection of information, including suggestions for reducing this burden, to Washington Headquarters Services, Directorate for information Operations and Reports, 1215 Jefferson Davis Highway, Suite 1204, Arlington, VA 22202-4302, and to the Office of Management and Budget, Paperwork Reduction Project (0704-0188), Washington, DC 20503

1. AGENCY USE ONLY (Leave blank)	2. REPORT DATE	3. REPORT TYPE AND DATES COVERED
	4 September 1990	Scientific Interim

4. TITLE AND SUBTITLE
Laboratory Study of the Thermochemical Properties of Materials Used in Spacecraft

5. FUNDING NUMBERS
PE 62101F
PR 7601 TA 30 WU 06

6. AUTHOR(S)
Terry L. Thiem, Lt, USAF
Lyn R. Watson
Rainer A. Dressler
Richard H. Salter
Edmond Murad

7. PERFORMING ORGANIZATION NAME(S) AND ADDRESS(ES)
Geophysics Laboratory (PHK)
Hanscom AFB
Massachusetts 01731-5000

8. PERFORMING ORGANIZATION REPORT NUMBER
GL-TR-90-0224
ERP, No. 1072

9. SPONSORING/MONITORING AGENCY NAME(S) AND ADDRESS(ES)

10. SPONSORING/MONITORING AGENCY REPORT NUMBER

11. SUPPLEMENTARY NOTES

12a. DISTRIBUTION/AVAILABILITY STATEMENT
APPROVED FOR PUBLIC RELEASE; DISTRIBUTION UNLIMITED

12b. DISTRIBUTION CODE

13. ABSTRACT *(Maximum 200 words)*

A high temperature mass spectrometer used to obtain laboratory data on the thermochemical properties of materials encountered in space research is described in detail. The experimental procedures and data analysis necessary to obtain thermochemical constants from the mass spectrometer data are also described. The present experimental arrangement allows cell temperatures of up to 2100 K. Reliable measurements at signal levels below 10 ion counts/s can be made because of the very low background signal and the entirely automated data acquisition and averaging system. In preliminary studies of osmium and its oxides, it is shown that the choice of molybdenum as the cell material is detrimental. The use of an alumina Knudsen cell is proposed.

14. SUBJECT TERMS		15. NUMBER OF PAGES
Materials	Thermochemistry	32
Space	Osmium oxides	16. PRICE CODE
Spacecraft	Mass spectrometry	
	High temperatures	

17. SECURITY CLASSIFICATION OF REPORT	18. SECURITY CLASSIFICATION OF THIS PAGE	19. SECURITY CLASSIFICATION OF ABSTRACT	20. LIMITATION OF ABSTRACT
Unclassified	Unclassified	Unclassified	SAR

Preface

This report describes a high temperature mass spectrometer located in the Spacecraft Interactions Branch. The apparatus is used to measure thermochemical properties of materials used in space research. Since its first operation, important modifications have been carried out on the instrument, such as acquisition automation, improved vacuum system, and improved ion detection efficiency. The instrument in its present state is described in detail with emphasis on the recent modifications.

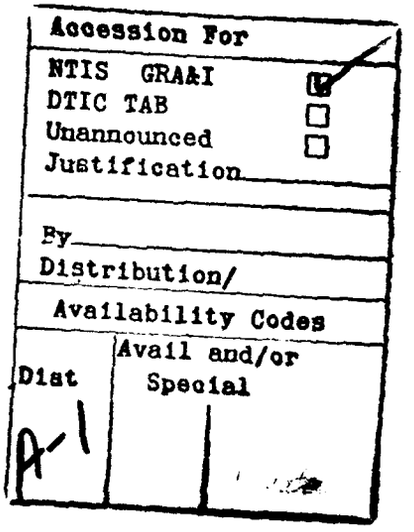

Contents

Illustrations

Laboratory Study of the Thermochemical Properties of Materials Used in Spacecraft

1. INTRODUCTION

Materials used in low earth orbit space flights are exposed to a harsh environment. Oxygen atoms are the main constituent of the atmosphere at low-earth-orbit altitudes of 200-400 km. At the orbital velocity of approximately 7.7 km s^{-1}, oxygen atoms collide with surfaces perpendicular to the velocity vector at a mean kinetic energy of 4.9 eV. Studies of materials subjected to this environment have indicated that these atom-surface collisions result in effects similar to those observed in laboratory studies of high-temperature vaporization and oxidation.[1,2] In these studies some materials are found to have gained mass, whereas others are found to have eroded or disappeared completely. The mass gain has been shown to be due to the formation of oxide coatings. The products formed when material is lost have not been identified. The mass loss may be due to: i) the formation of highly volatile reaction products; ii) the distribution of the excess reaction energy to the material lattice, resulting in subsequent vaporization of reaction products or unreacted material; or iii) chipping of surface materials, particularly thin films.

To understand and predict the extent of these interactions, it is necessary to develop models of the vaporization or decomposition processes. A prerequisite for such models is knowledge of the reaction energetics. These can be derived from thermochemical properties of the reactants and products such as heats of formation and bond dissociation energies. The thermal conductivity and the heat capacity of the material determine how the excess reaction energy is absorbed and whether vaporization occurs.

In many instances, the thermochemical properties of possible reaction products such as metal oxides are not accurately known. For example, osmium (Os), frequently used as an optical coating due to its high VUV reflectivity, has been observed to disappear completely during space shuttle flights.[3] Of the osmium oxides, accurate thermochemical data is known only for OsO_4, which is stable at high temperatures. It is conceivable that formation of OsO:

$$Os(s) + O(g) \rightarrow OsO(g) \qquad (1)$$

is responsible for the loss of osmium. Only rough estimates of the heat of formation of OsO exist.[4] By measuring for example the heat of reaction for the process

$$2\ Os(g) + O_2(g) \rightarrow 2\ OsO(g) \qquad (2)$$

the heat of formation as well as the dissociation energy of OsO could be determined.

(Received for publication 12 September 1990)

In the past 30 years, high-temperature effusion beam mass spectrometry has proven to be an invaluable tool in the study of high temperature reaction equilibria.[5] In these experiments, vapors composed of gases in a chemical equilibrium effuse from a hot cell. This cell is generally referred to as a Knudsen cell. The effusive beam is then ionized, accelerated and dispersed through a magnetic mass analyzer for identification. In a correctly calibrated instrument, the measured abundances of the species present in the beam yield the respective partial pressures in the Knudsen cell, which enable the determination of the equilibrium constant K of the reaction being investigated.

Thermochemical data such as the heat of reaction of a chemical process can be obtained from measured equilibrium constants through thermodynamic expressions based on the Second and Third Laws of Thermodynamics. One generally differentiates between second- and third-law heats of reaction. Second-law heats of reaction can be obtained from the van't Hoff equation:

$$\Delta H^\circ = - \frac{d(R \ln K)}{d(1/T)} \tag{3}$$

where ΔH° is the standard reaction enthalpy or heat of reaction at the temperature T, and R is the ideal gas constant. When plotting $-(R \ln K)$ against $1/T$ (the van't Hoff plot), the slope yields ΔH° at the midpoint of the temperature range investigated. However, the variation of ΔH° with temperature is a possible source of error in the equilibrium constant determined using this method. Furthermore, ΔH°_{298}, the standard heat of reaction at 298.15 K, can frequently only be obtained through extrapolation from high temperature data. A strong dependence of ΔH° on temperature therefore results in a significant error when determining this value.

Third-law heats are obtained by use of the *free energy functions* of each reaction component. The free energy function, $(F^\circ_T - H^\circ_0)/T$, is a linearized form of the entropy, and can be calculated precisely using statistical mechanics if the energy levels and symmetries of the low-lying states of the molecules are known from spectroscopic data. The heats of reaction are then obtained from Eq. (4):

$$\Delta H^\circ_0 = T \left[\frac{\Delta F^\circ_T}{T} - \Delta \left(\frac{F^\circ_T - H^\circ_0}{T} \right) \right] \tag{4}$$

where ΔH°_0 is the standard reaction enthalpy at 0 K and ΔF°_T is the standard free energy of the reaction at a temperature T and is obtained from:

$$\Delta F^\circ_T = -RT \ln K \ . \tag{5}$$

Equation (4) can also be rewritten to yield ΔH°_{298} if the free energy functions $(F^\circ_T - H^\circ_{298})/T$ have been determined.

In contrast to the second-law method, the third-law method can be used to calculate the heat of formation at a standard temperature from each individual equilibrium constant measured. Whenever possible, it is useful to calculate standard reaction enthalpies using both methods for comparison of the values obtained. For example, the third-law values can reveal curvature in the van't Hoff plot used to determine the second-law value. This curvature could otherwise remain undetected. However, if spectroscopic measurements or theoretical calculations are not available for the states of the molecules of concern, then the free energy functions can not be calculated precisely and heats of formation can be determined only by the second-law method.

In Section 2 of this report, the technical aspects of the high temperature mass spectrometry experiment are described. The various measurement modes used to calibrate the experiment as well as identify reaction products are described in Section 3. Preliminary work on the oxidation reactions of Os is presented in Section 4. In Section 5, conclusions are drawn and improvements are suggested.

2. INSTRUMENTATION

2.1. Overview of the Apparatus

The apparatus consists of a Nuclide high temperature mass spectrometer (model 12-60), which is shown schematically in Figure 1. It is evacuated using 4 and 8 inch diameter cryopumps

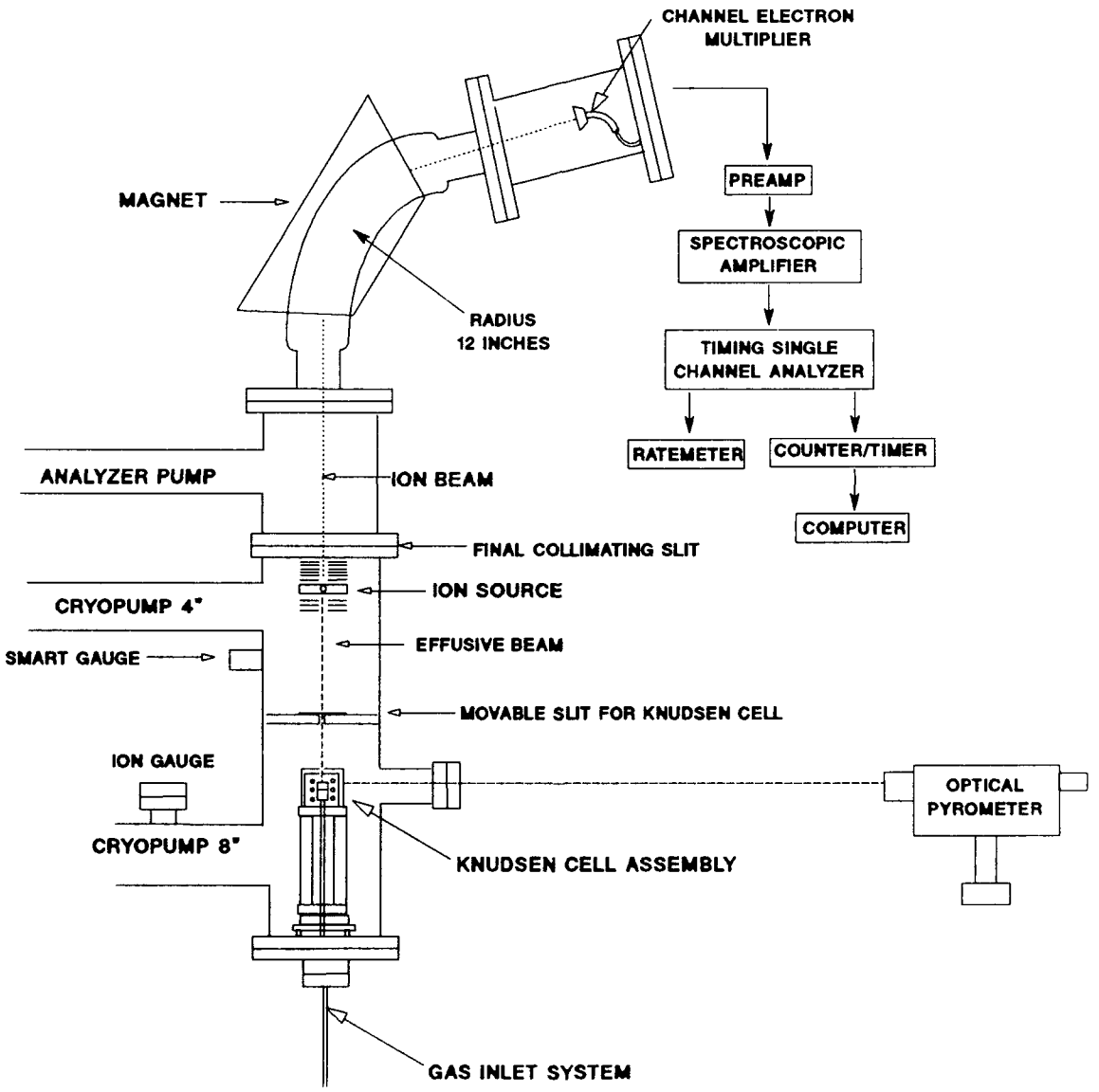

Figure 1. Schematic Diagram of the High Temperature Mass Spectrometer

(CTI Cryogenics) and one 4 inch ion pump (Varian). An effusive beam emanates from a Knudsen cell containing vapors of a high temperature equilibrium. The temperature is measured by optical pyrometry or by thermocouples. Atoms or molecules of the beam are ionized when they pass through an electron impact ion source. The resulting ion beam is accelerated into a 12 in. radius, 60° magnetic sector mass analyzer. The selected ions are then detected by a channel electron multiplier. The output of the detector is amplified and discriminated, and the resulting pulses are counted. The acquired signals are stored and processed by an AT-compatible computer. Below is a description of the major components of the instrument.

2.2. Knudsen Cell

2.2.1. KNUDSEN CELL ASSEMBLY

The Knudsen cell assembly, shown in Figure 2, consists of the Knudsen cell itself, a heating coil, radiation shielding, a movable shutter, and an adjustable entrance slit to the ion source. One version of the cell is equipped with a gas inlet tube. The Knudsen cell is heated radiatively by a tantalum or tungsten heating coil. By resistively heating the coil with a current of up to 200 A, a

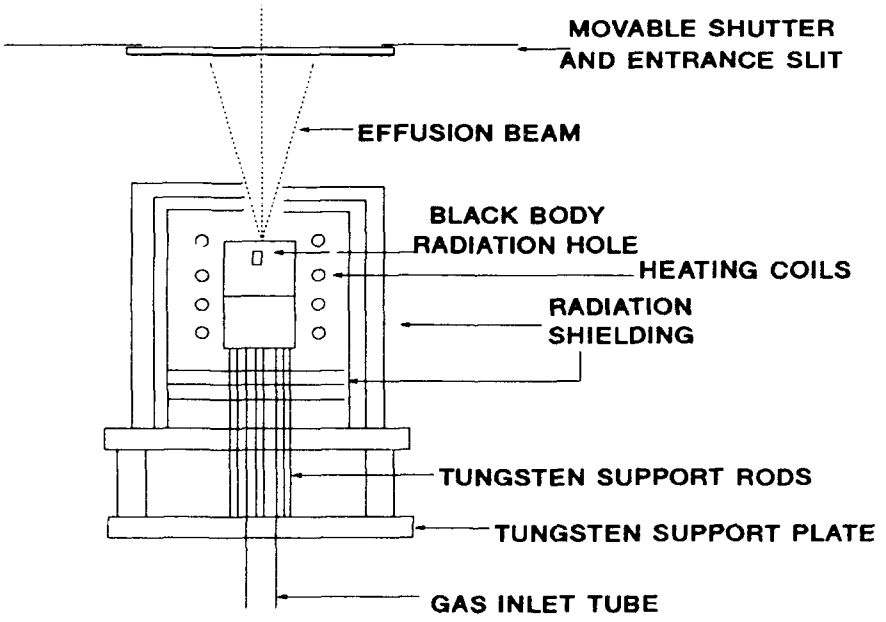

Figure 2. Schematic Diagram of the Knudsen Cell Assembly

maximum cell temperature of 2100 K can be obtained. Radiation shielding made of tantalum in sheet form is used to contain the heat in the Knudsen cell area thereby avoiding excessive heating of the vacuum chamber walls. A circulating water jacket aids in the dissipation of heat from the chamber walls surrounding the Knudsen cell and the leads to the heating coils. The Knudsen cell is cylindrical and has a length of 1 in., an outer diameter of 1/2 in., and an internal diameter of 5/16 in. Because the ratio between the area of the effusion orifice and the area of the vaporizing sample is small, effusion from the orifice does not perturb the equilibrium between the gaseous and condensed phases. The cell material must withstand high temperatures and is usually molybdenum, tungsten, or alumina. The effusion orifice is located in the top center of the cell and is 1 mm in diameter. The black body cavity for temperature determination is drilled into the side of the cell near the top face in such a way that the internal chamber is not penetrated. Temperature measurement is described in the next section.

2.2.2. KNUDSEN CELL TEMPERATURE MEASUREMENT

The temperature of the Knudsen cell is measured either by thermocouples or by optical pyrometry. In the latter technique, the temperature is determined by measuring the radiation emanating from a black body cavity in the Knudsen cell.

A black body is an ideal emitter (or absorber) of radiation. Objects emit electromagnetic radiation with an intensity and a wavelength distribution that depends on the temperature of the object. A black body is ideal because it emits (and absorbs) all frequencies of radiation in a uniform way.[6] A small isothermal cavity with a length to diameter ratio of at least 10 closely approximates the absorbing and emitting properties of a black body. By measuring the intensity of radiation (in a narrow spectral range) from such a cavity in the Knudsen cell, the temperature of the Knudsen cell (that contains the hole) can be determined.

The instrument used to measure the radiation from the Knudsen cell cavity is an optical pyrometer (The Pyrometer Instrument Co.) that consists of an optical system and an electronic system. The position of the pyrometer with respect to the high temperature cell is shown in Figure 1. The optical system collects radiant light from both the target and an internal reference lamp. The intensities of these two beams are compared by alternate focusing onto a photomultiplier tube. A vibrating reed provides the modulation for this alternate focusing. As the two beams are being compared, the electronic system adjusts the current supplied to the reference lamp until the two beams are of equal intensity. This current is the output of the pyrometer. The signal is read by measuring the potential drop across a built-in standard 5 Ω resistor. The temperature that corresponds to the output signal is determined from a calibration curve, which is made by focusing the pyrometer on a target of known temperature [a ribbon filament strip lamp (The Pyrometer Instrument Co.)] and recording the output.

Thermocouples are also used to measure the temperature of the Knudsen cell. Four types of thermocouples are used, depending on the temperature range being measured. Type K, the chromel/alumel pair, is used between 700 and 1000 °C. Type S, the platinum/platinum 10% rhodium pair, is used up to 1500 °C. Type B, the platinum 6% rhodium/platinum 30% rhodium pair, is used up to 1700 °C. Finally, Type C, the tungsten 5% rhenium/tungsten 26% rhenium pair, can be used to 2300 °C in non-oxidizing atmospheres. All thermocouple wire was purchased from Omega Engineering and junctions are made by spot welding.

The thermocouple junction is positioned on the side of the Knudsen cell near the black body cavity and is held in place by tungsten wire. Placement of the junction is important for the measurement of the true equilibrium temperature In addition, the accuracy of temperatures measured using thermocouple junctions is affected by the details of the thermocouple installation. Therefore the thermocouple wire is continuous to the outside of the vacuum chamber. This is accomplished by hard-soldering the wire into the thermocouple feedthrough tubes of a vacuum flange. This arrangement precludes any errors that would be introduced by the presence of additional junctions inside the vacuum chamber where temperature gradients exist. The thermocouple leads are connected to the read-out device by lengths of insulated extension grade wire appropriate for each thermocouple type.

The voltage difference between the legs of the thermocouple is measured using a digital thermometer (Fluke) that has an internal junction referenced to 0 °C. The output of the thermocouple can therefore be displayed in degrees Celsius or can be read directly in mV.

2.3. Ion Source

The chamber that contains the ion source is evacuated by the 4 inch cryopump that has a pumping speed of 250 *l*/s. The cryopump has a pumping speed approximately 4 times greater than a previously-used ion pump. Pumping speed is further increased over the former arrangement because the cryopump is mounted directly onto the chamber whereas the ion pump was separated from the chamber by a long tube with a 90° bend. The new pump decreases the background pressure in the ion source to a level that does not interfere with the measurement of reactant count rates. Prior to the pump replacement reactant gases such as oxygen could not be discerned from background gases.

The size of the atomic or molecular beam entering the ion source is defined by the slit to the ion source. A movable shutter placed above this slit allows the beam to be distinguished from background gases.

The ion source assembly used in this experiment is shown in Figure 3. The ion source consists of collimating plates, a repelling electrode, an electron impact ionization source including a filament (located in J1) and an electron trap, and eight other accelerating and focusing plates, J2-J9, in the accelerating region.

2.3.1. IONIZATION REGION

The effusive molecular beam enters the ion source through the Knudsen cell shutter. There are four plates above the shutter, a collimating, an ion suppression, another collimating, and a repeller electrode. The first collimating plate and the ion suppression electrode (a split pair) are connected to J1 and are at full ion acceleration potential. This potential serves to reject any ions in the molecular beam. The second collimating plate supports the electron trap (described below) and is at trap potential. The repeller plate potential is optimized for ion extraction and is typically 1-2 V.

Ions are formed by an electron impact ion source. The molecular beam is crossed at right angles by an electron beam emitted from a hot filament (located on J1 as stated above) through thermionic emission. The emission current is set to 0.8 mA as a compromise between emitted electron density and filament lifetime. We are using thoriated iridium ribbon as filament material because of its durability and electron emitting characteristics. The primary and secondary electrons are collected by an electrode which is called the electron trap.

A trap potential of 40 V with respect to the shield potential produces the maximum trap current. The trap current is a measure of the electron current that actually passes through the ionization region. The same emission current can yield different trap currents depending on the location of the filament with respect to the shield aperture. Therefore the filament position is critical to the trap current. It has been found experimentally that the trap current is maximized when the center of the filament is about 1 mm away from the first electron acceleration plate.

The number of positive ions produced by the electron beam is directly proportional to the density of gas molecules at pressures below 10^{-4} torr. Positive ions are accelerated by a potential difference applied between the ion source and the mass filter, which is at ground potential. The ionization region (shield plate) is typically held at 4500 V. Lower accelerating voltages significantly decrease the sensitivity and the resolution of the instrument.

The filament is heated by a direct current which is controlled by an emission-current regulating circuit described below. The circuit adjusts the filament heating current to the value necessary to produce the emission current set by the user. The potential difference between the midpoint of the filament and the shield electrode determines the electron energy, provided the repeller electrode potential is low. Higher repelling fields provide higher sensitivities, but lead to ionization in a non field-free area, thus affecting the electron energy and the electron energy resolution.

2.3.2. ACCELERATION REGION

The ions produced in the shield area (J1) are accelerated successively from electrodes J1 to J9. Plates J2 and J3 are defocusing and discriminating slits, respectively. J4 and J5 are a split pair used to deflect and focus the ion beam. Plate J6 is a collimating (beam-width defining) slit.

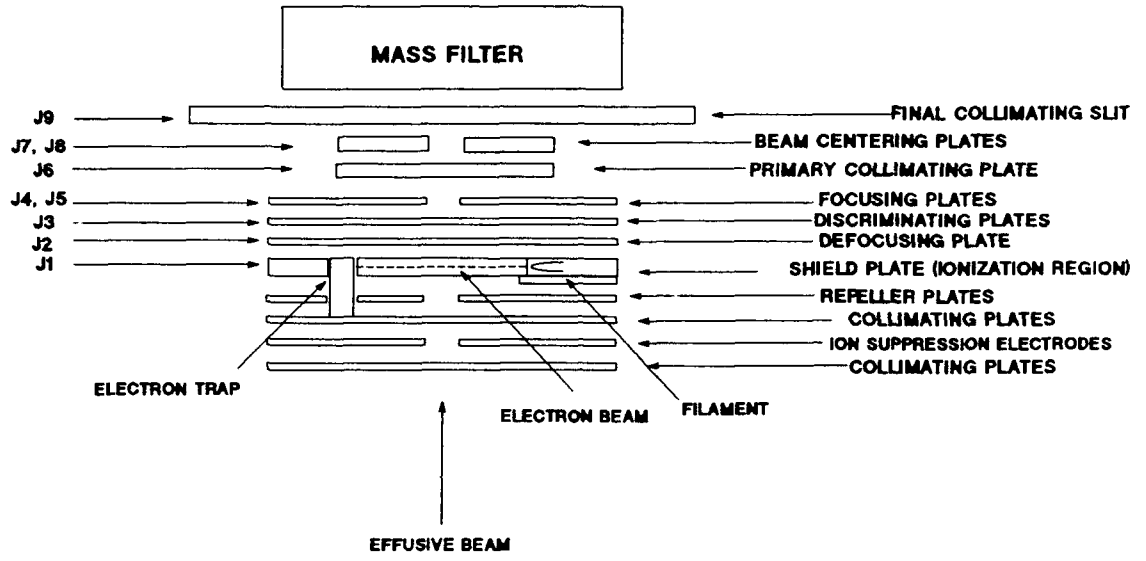

Figure 3. Schematic Diagram of the Ion Source Assembly

Plates J7 and J8 are also a split pair and are used for deflecting the ion beam into the J9 slit. Plate J9 contains the final object-defining slit for the mass filter. Its width determines the resolution of the mass spectrometer and is adjustable from outside of the vacuum system by means of a micrometer.

2.3.3. ELECTRODE POTENTIAL CONTROL

Voltages applied to J1-J9 and the first two collimating plates in the ion forming region are obtained through a Nuclide Model HV-21 high voltage power supply and are controlled through a Nuclide SC-5D source divider. Typical voltages on the accelerating plates are: J1, full ion accelerating potential, usually 4500 V; J2, zero to 400 V below J1; J3, zero to 400 V below J2; J4-J5, 400 to 4000 V below J1; J6, true ground; J7-J8, zero to 120 V (negative electrode at true ground); J9, true ground.

The Nuclide ER-11 emission current regulator and electron energy selector control the electron energy, the emission current of the filament (electron current), the repeller potential, and the electron trap potential. The electron energy can be controlled through the electron energy selector but in practice is controlled digitally by the computer through a D/A converter floating at the acceleration potential. The electron energy can be varied from nearly 0 eV to 81.915 eV.

The filament emission current control is accomplished by a feedback circuit that adjusts the voltage across the filament to maintain a constant emission current which is preset by the

experimenter. The emission current is equal to the current between the filament bias supply and the filament current supply. The filament current can be limited to avoid overheating of the filament under conditions which cause inefficient emission, such as a sudden drop to very low electron energies.

The computer interface and control parameters for the electron energy are described in the Data Acquisition Section 2.6.

2.4. Mass Analyzer

After passing through the object defining slit in plate J9, the beam enters the mass analyzer. Mass analysis is accomplished using the properties described below[7].

An ion moving at right angles to the direction of a uniform magnetic field is subject to a force **F**

$$\mathbf{F} = e\mathbf{v} \times \mathbf{B} \tag{6}$$

where e is the ion charge, **v** is the ion velocity, and **B** is the magnetic field strength. The vector product indicates that the magnetic force is always perpendicular to both the magnetic field and the direction of motion of the particle. This results in a circular motion for an ion moving at constant velocity. The force on the ion causing this circular motion is equal to the mass of the ion multiplied by the centripetal acceleration:

$$e\mathbf{v} \times \mathbf{B} = mv^2/r \tag{7}$$

where m is the mass and r is the radius of the circular motion.

The kinetic energy of the ion, E, is given by:

$$E = mv^2/2 = eV \tag{8}$$

where V is the accelerating potential. Rearranging Eqs. (7) and (8) and solving for m/e one obtains:

$$m/e = (r^2 \bullet B^2)/2V \tag{9}$$

For a fixed radius of curvature and accelerating potential, the mass-to-charge ratio is directly proportional to the square of the magnetic field. In the high temperature mass spectrometer, the ion acceleration potential is constant at 4500 V, as previously stated, and masses are selected by varying the magnetic field.

The magnetic field is varied using the magnet regulator (Nuclide Model No. MR-13). The transmitted mass-to-charge ratio can be controlled either directly by adjusting the magnet current, or indirectly by adjusting the induction. The induction is measured using a temperature-regulated Hall probe. The induction is adjusted by setting a reference voltage. The circuitry of the Nuclide MR-13 magnet regulator then provides the magnet current necessary for the Hall voltage to equal the preset reference voltage. The induction control has the advantage of overcoming reproducibility problems associated with the hysteresis of the ferro-magnetic poles.

At the greatest magnetic field attainable in the instrument, 1.5 Tesla, ions with mass-to-charge ratios of 2000 a.m.u. per charge can be transmitted when the ion acceleration potential is

4500 V. Higher masses can be transmitted at lower acceleration potentials at the expense of sensitivity and resolution. The mass resolution of the instrument ($m/\Delta m$) can be as high as 1500 depending on the width of the final (collector) slit. The collector slit width for a typical experiment yields a resolution of about 350 (peak width definition at 5 percent of peak height). The larger slit width provides greater sensitivity but reduces resolution.

For the application being described here, the advantage of the magnetic sector instrument over the more compact and less expensive quadrupole is the larger mass range available and the superior resolution.

2.5. Ion Detection

Ions that have passed through the 60° magnetic sector and the exit slit (adjustable by micrometer from outside the vacuum) are accelerated by a negative 2200 V potential applied to the cathode of a channel electron multiplier (Galileo Electro-Optics Corp.). Channel electron multipliers are heavily lead-doped, horn-shaped glass tubes with secondary emissive and resistive characteristics. In contrast to the more traditional discrete-dynode electron multipliers containing several dynodes, the channel electron multiplier consists of a single continuous dynode surface within the glass tube. A potential applied across the tube will result in a continuous voltage gradient within the tube. Secondary electrons are produced by ions striking the surface and are accelerated within the tube, thus gaining energy which enables these electrons to create further secondary electrons upon hitting the channel surface.

The most important advantages of channel electron multipliers over discrete-dynode multipliers are: low dark count rates; a stable dynode surface which is insensitive to atmospheric exposure; narrow gain distribution of output pulses; lower bias voltages and currents; and smaller physical size. The detection efficiency is addressed in Section 3.3.3. The multiplier in this work is a high current Channeltron which can be operated in either a pulse counting or analog mode. The detector generates pulse heights greater than 100 mV at a bias voltage of 2200 V.

2.6. Data Acquisition

2.6.1. DATA ACQUISITION HARDWARE

The data acquisition hardware configuration is shown in Figure 4. It is similar to the one described by Gardner et al.[8] The data acquisition hardware consists of signal processing electronics and an AT-compatible computer with a counter/timer and a digital to analog converter, which enable multichannel scaling. The negative pulses from the ion detector are passed through a fast preamplifier (Stanford Research Systems, Inc) located directly at the ion signal vacuum feedthrough. The preamplifier matches the detector output impedance to the receiving amplifier input impedance of 50 Ω. The pulses are amplified and shaped to positive pulses by a spectroscopic

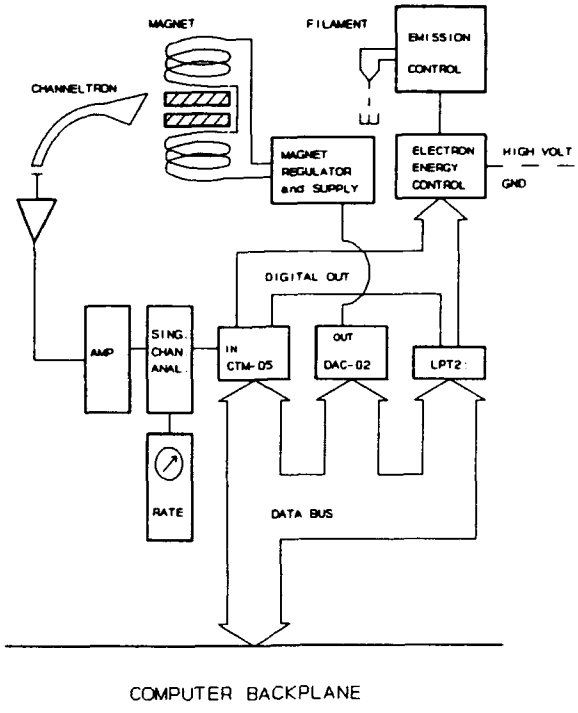

Figure 4. Schematic Diagram of the Data Acquisition Hardware

amplifier. The amplifier output is further processed by a single channel analyzer that is used as a discriminator. The single channel analyzer converts input pulses exceeding a set voltage level to TTL pulses. At normal detector bias voltages, pulse heights resulting from ion detection far exceed noise levels. The noise count rates are therefore extremely low, and are primarily given by the dark count rate of the detector, which is specified to be below 0.5 count per second.

The single channel analyzer output is connected to a ratemeter and the counter-timer interface in the AT-computer. In the ratemeter, the ion pulses are converted to an analog signal through an RC network. The sole purpose of the ratemeter is visualization of the count rate.

The TTL output of the discriminator is fed into the input of one counter on a counter-timer computer interface card (Metrabyte CTM-05). A timer is programmed to produce a constant square wave signal which is connected to the count-enable gate of the signal counter. The length of the count-enable pulse (dwell time) is predetermined by the user and is well defined. The microprocessor has access to the latches in the counters, from which the data can be read.

When the experiment requires scanning of the magnetic field strength (mass scan), a voltage ramp must be generated. A 12-bit digital-to-analog (DAC) converter computer interface card

(Metrabyte DAC-02) with an output range of 0 to +10 V is used. The digital input of the DAC, provided by the computer, is incremented following each count period. The resulting analog output of the DAC is adjusted by the variable resistor of a summing amplifier network. The variable resistor allows the total scan range to be varied. The ramp is then added to the mass scan offset voltage of the inductance control circuitry. The amplifier and the feedback circuit then produce whatever output is necessary to make the Hall voltage equal to the reference voltage.

When the experiment requires sca. .ning of the electron energy a voltage ramp which floats at the ion source acceleration potential must be generated . In this case, the computer produces a 12-bit digital output by combining an output port of the CTM-05 interface card and the 8 bit LPT2: parallel port. This output is connected to the digital input of the Nuclide electron energy control unit, where the digital data lines are coupled to the ion source high voltage through opto-isolators. The analog ramp is then generated with a digital-to-analog converter floating at the acceleration potential. The digital-to-analog converter allows a maximum scan range of 81.92 V, corresponding to a digital input of 4095 with 20 mV/channel.

2.6.2. SOFTWARE

The AT computer and the interface cards are programmed to operate as a multichannel scaler. The role of the multichannel scaler software is to:

1. Accept the data acquisition parameters and control commands of the user.
2. Read the counter and store the counts in memory.
3. Control the experiment by driving the digital-to-analog converters.
4. Display the experimental data during acquisition.
5. Store the complete data onto a disk.
6. Manipulate the data and create hard copies.

The source code is a combination of FORTRAN 77, MACRO ASSEMBLER, and C routines. The main program is written in FORTRAN, the computer interfaces are controlled with ASSEMBLER, routines and color graphics routines are written in C. During acquisition, the program reads the counter contents, adds the acquired counts to the memory location of the current channel, increments the digital output to the DAC, and reads the keyboard for commands. There are four possible acquisition modes:

1. Regular mass scan
2. Linear mass scan
3. Segmented mass scan ("peak hopping")
4. Electron energy scan.

In the regular mass scan mode, the digital input to the DAC is incremented by a fixed amount following each count period. Since m/e is proportional to B^2 [Eq. (9)], the X-axis of the mass spectrum will not reflect a linear mass scale. A linear mass scale can be obtained if the digital ramp

is incremented according to a square root function. This square root function is given by the equations:

$$A(i) = C\bullet[\{m_o + (i-1)(m_f - m_o)/N\}^{1/2} - (m_o)^{1/2}] + B \quad (10)$$

$$A(1) = 1 \quad (11)$$

$$A(N) = 4096, \quad (12)$$

where A(i) is the integer DAC input for channel i, N is the number of channels, C and B are constants, and m_o and m_f are the first and the last masses of the mass spectrum. Solving for B and C, one obtains for large N (N > 100):

$$B = 1$$

$$C \approx 4095/\{(m_f^{1/2} - (m_o)^{1/2}\}. \quad (13)$$

Each data channel is assigned a DAC input number [A(i)] prior to the first mass scan. Instead of incrementing the DAC by a constant number between count periods, the program transfers the particular A(i) to the DAC input register.

When determining intensities of particular masses in a mass scan, one normally encounters large segments of the mass spectrum where no signal of interest is observed. Consequently, much of the acquisition time is actually wasted. This can be circumvented by narrowing the mass scan down to a few segments containing the peaks of interest, thus reducing the acquisition time considerably. The software enables the definition of an unlimited amount of segments. During a mass scan, the multichannel scaler hops from one segment to another, omitting acquisition in areas where intensities need not be measured.

To scan the electron energy at a particular mass, the computer is programmed to write the low byte of the 12-bit digital ramp number to the output port on the CTM-05 interface card and the high nibble to the LPT2: parallel port.

3. INSTRUMENT CALIBRATION

3.1 Mass Calibration

The purpose of mass calibration of the instrument is to determine the magnetic field that will transmit an ion of a given mass-to-charge ratio. Although in theory Eq. (9) can be used to calculate the magnetic field necessary to transmit an ion of a particular m/e ratio for a given ion acceleration potential, in practice the equation is not accurate. Magnetic fields, like electric fields, do not have well-defined boundaries. Therefore the exact value of *r*, the radius of curvature, is unknown. Imperfections in the alignment of the instrument can also affect the focusing characteristics. Therefore it was necessary to experimentally determine the "effective radius" of the instrument. This was done by determining the magnetic field necessary to focus ions of known mass and charge. The effective radius is then calculated using Eq. (9) since the other variables in the equation are of known value. By using the effective radius and Eq. (9), the magnetic field necessary to focus a particular ion can be accurately calculated.

For the low mass region, below 50 a.m.u., the background gases H_2O, N_2 , O_2 , and CO_2 were used as the standards. For the high mass region, xenon was used because of its molecular weight and large number of isotopes. A mass spectrum of xenon is shown in Figure 5.

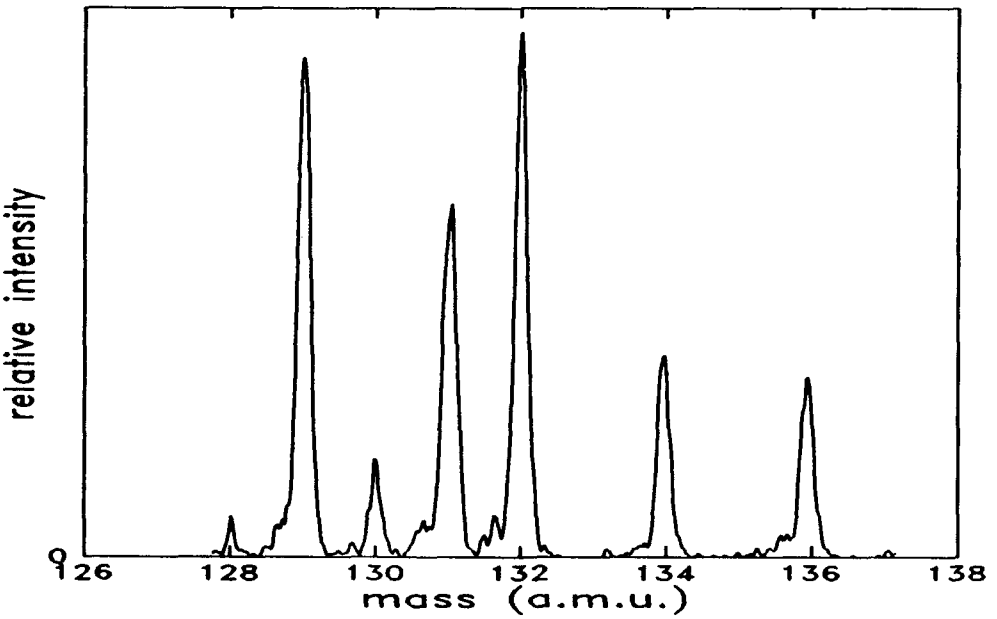

Figure 5. Mass Spectrum of Xenon

3.2. Knudsen Cell Density Calibration

The thermodynamic properties of a chemical process can be calculated from the equilibrium constant for that process. To determine this equilibrium constant using high-temperature mass spectrometry, it is necessary to relate the measured ion intensity to the vapor pressure inside the Knudsen cell. Calibration is conveniently performed by measuring the ion intensity resulting from the vaporization of a sample of known vapor pressure. Silver is commonly used as such a standard.[9] The result of such a calibration is an equation of the form:

$$P_i = P_{Ag} \frac{I_i T_i}{I_{Ag} T_{Ag}} C \tag{14}$$

where P, I, and T are pressure, ion intensity, and temperature, and C is the constant of proportionality. The subscripts refer to the vapor of unknown pressure (i) and to the standard of known pressure (Ag). The values for T and I are experimentally determined and the vapor pressure of silver at a given temperature, $P_{Ag}(T)$, is known from published vapor pressure versus temperature curves.[10] Once the value of the constant C is determined, the partial pressure of the compound being studied can be determined from Eq. (14).

The constant C is a function of the molecular beam characteristics, the ionization conditions and the detection efficiency of the particular ion. The effects of these components on the measured ion intensity and the proportionality constant C is presented below.

3.2.1. MOLECULAR BEAM CHARACTERISTICS

The effusive flux of molecules from a Knudsen cell is given by Graham's law[11]

$$Z_{eff} = \frac{\bar{c} P A_o}{4kT} \tag{15}$$

where $\bar{c}$ is the mean molecular speed, P is the equilibrium partial pressure, A_o is the area of the orifice in the Knudsen cell (equal to 0.8 mm^2 for the instrument being described), and k is the Boltzmann constant. From the Knudsen cell the effusive beam passes through an opening in the heat shield and through the shutter. Some portion of the beam then passes through the beam-defining slit into the ion source. The fraction of the effusing beam that reaches the ion source depends upon the geometry of the instrument, that is, the distance between the effusion orifice and the ion source, the position of the heat shield with respect to the orifice, the size and position of the shutter slit, and the size of the beam defining slit. For a given arrangement of the instrument

components, these factors are the same for both the calibrating vapor and the vapor being studied. Therefore these factors cancel out of the proportionality constant.

3.2.2. IONIZATION CONDITIONS

The fraction of the beam entering the ion source that is actually ionized depends on the current density and energy of the electrons and upon the ionization cross section of the atoms or molecules in the beam. The current density of the electron beam is a function of the filament material, the filament temperature, and the electron trap potential. These values are maintained for both calibration and measurements and therefore do not enter into the calibration constant. However, each time a filament is replaced, the new filament must be re-calibrated with silver.

The energy of the electrons is important because the cross-section for ionization of an atom or molecule, σ, is electron energy dependent. This is demonstrated in Figure 6,which shows the oxygen ion intensity versus electron energy curve. Ions appear at an electron energy of about 12 V (the appearance potential, AP) and the ion intensity increases linearly up to about 30 V at which energy some curvature appears in the plot. It should be noted that appearance potential plots are a useful indicator of the true electron energy when the appearance potential of the particular atom or molecule is known. The true electron energy may differ from the set electron energy due to interference from the repelling voltage if it is too high, as mentioned above. (Recall that the repelling voltage is used to "draw out" or direct the positive ions to the appropriate path.)

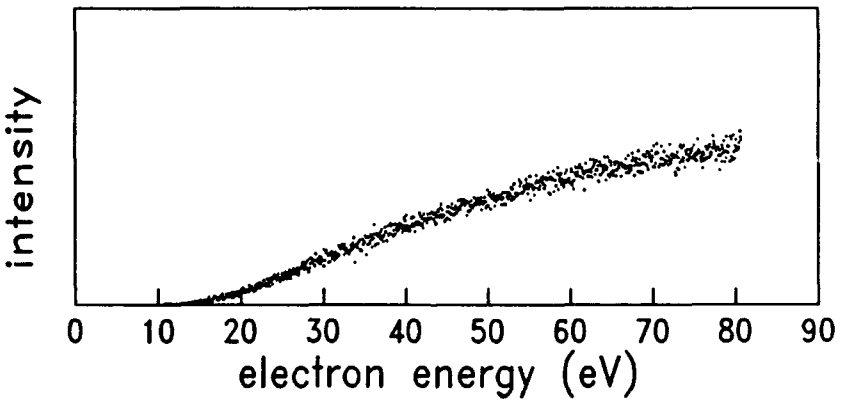

Figure 6. Appearance Potential for Oxygen

The choice of electron energy for monitoring the neutral number during an experiment merits some discussion. Although maximizing the electron energy yields higher ion currents, it is

useful and sometimes necessary to work with lower energy electrons to avoid dissociative ionization or multiple ionization of molecules. Also, ionization of an interfering species can sometimes be avoided by the judicious choice of electron energy. The cross-section of each atom or molecule must be estimated for the appropriate electron energy. The maximum value of the cross-section, σ_{max} , has been calculated for many atoms by Otvos and Stevenson.[12] Those authors have also postulated that the ionization cross-sections of molecules can be found by adding the σ_{max}'s of the component atoms. This approach has been generally accepted.[5] Once σ_{max} is calculated, the ionization cross sections at different energies, σ_E , can be determined. As seen in Figure 6, there is a region of linear increase in ionizing efficiency above threshold. Following Drowart and Goldfinger[5], within this linear region, σ_E for a given species is estimated by the equation:

$$\sigma_E = \sigma_{max} (E\text{-}AP)/(E_{max} - AP) \tag{17}$$

where E is the energy of σ_E and E_{max} is the energy of σ_{max} . In cases where E_{max} is not directly measurable because of molecular fragmentation or other limitations, the value $E_{max} - AP$ is assumed to be approximately constant. The σ_E's so determined are one component of the calibration constant, namely $C \propto \sigma_{Ag} / \sigma_i$.

3.2.3. ION DETECTION EFFICIENCY

The detection efficiency of the multiplier for a particular ion is the ratio of the number of pulses per unit time to the number of impinging ions per unit time in percentage form. The detection efficiency of the channel electron multiplier is known to be mass dependent.[13] The mass dependency is strongest at low ion energies. The instrument being described here, the ions are accelerated in the ion source by the 4.5 kV acceleration potential. When combined with the highly negative multiplier input potential (-2.2 kV), the ions are accelerated by a total of nearly 7 kV. At such high energy levels the detection efficiency has been observed to plateau at a high level.[11] For example, for 4 keV neon ions and a bias voltage of -2.8 kV, the detection efficiency is approximately 90 percent. Therefore, no correction for detection efficiencies is necessary in this work.

Another possible source of error is the fragmentation of larger molecules upon collision with the detector surface. This would in effect increase the gain of the multiplier. However, the count rate observed would not be affected by such an increase in gain, since a single count results from such processes. Therefore the detector characteristics only negligibly affect the proportionality constant C.

Thus the density calibration, in its final form, is

$$P_i = P_{Ag} \frac{I_i T_i \sigma_{Ag}}{I_{Ag} T_{Ag} \sigma_i} \quad . \tag{16}$$

4. PRELIMINARY RESULTS

4.1 Density Calibration

The density calibration of Eq. (16) is the first step of an experiment. Such a calibration was made and the results are shown in Figure 7 in the form of a van't Hoff plot. The heat of sublimation for silver calculated from the slope of the line shown in the figure is 71.4 ± 5.4 kcal/mol. The error is 3σ, calculated from a standard least-squares linear fit to the data. This is somewhat higher than the known value of 66.7 kcal/mol (median value for the temperature range of 800 to 1230 K)[14] and is probably due to problems in measuring the temperature accurately. However, the true value is within 3σ of our measured value.

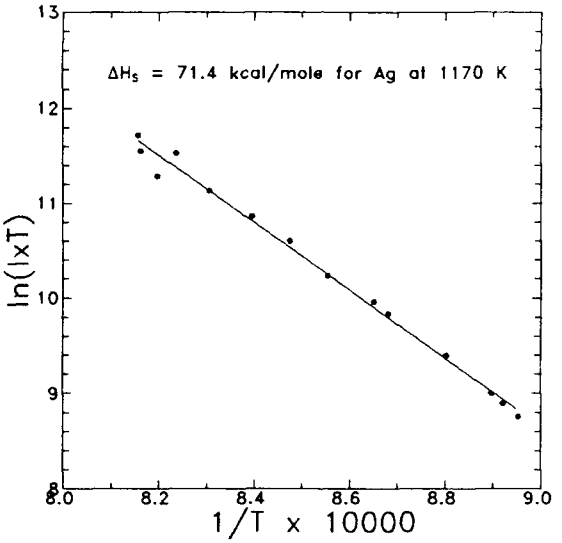

Figure 7. van't Hoff Plot for Silver

4.2 Osmium Oxide Studies

Following the calibration of the instrument, the osmium-oxygen system and in particular the equilibrium

$$OsO_4(g) \rightarrow OsO_3(g) + 1/2\ O_2(g) \qquad (18)$$

was studied. Reaction (18) has previously been studied by Grimley et al.[15] in 1960 but has not been studied since. In addition to studying Reaction (18), Grimley et al. also looked for the presence of the lower two oxides. They did not detect the presence of OsO_2 under the conditions of their experiment.

Our first approach was to use a molybdenum Knudsen cell with an oxygen inlet. Powdered osmium was placed inside the cell and oxygen gas was passed through the metal sample as the cell was heated. The oxygen pressure was on the order of 10^{-5} atm. We detected both OsO_3 and OsO_4 using this method. An appearance potential measurement for OsO_3 is shown in Figure 8. Osmium trioxide ions begin to appear well below 15 eV, which demonstrates that the parent molecule was OsO_3 and not OsO_4 : for the OsO_3 signal to be due to fragmentation of OsO_4 , an electron energy of at least 17 eV is required.[16] However, we were unable to obtain the second-law van't Hoff plot for Reaction 18 because of the interfering formation of molybdenum dioxide dimer at about 1200 K. The molybdenum oxides formed from the reaction of oxygen gas with the Knudsen cell precluded a systematic study of the osmium-oxygen equilibrium.

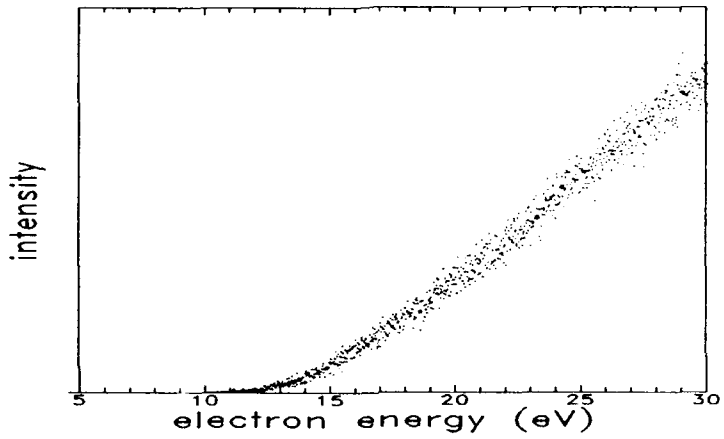

Figure 8. Appearance Potential for OsO_3

As an alternative to the molybdenum cell, we used an alumina Knudsen cell that was available in the laboratory but that was not equipped with an oxygen inlet. A mixture of powdered osmium and Cr_2O_3 was placed in the alumina crucible. The chromium oxide was intended to act as an oxidizing agent for the formation of osmium oxides. Under these conditions we obtained a spectrum of all four of the osmium oxides as shown in Figure 9.

The four largest peaks in each oxide group are attributable to the four most abundant isotopes of osmium. The spectrum was obtained at 700 K and an electron energy of 80 eV. The measured appearance potential of the OsO_3 present under these experimental conditions, about 12.3 eV, indicates that it was not all formed as an electron impact fractionation product of OsO_4 , which would require an energy of 17eV, as noted above. There is also an indication that some small fraction of the OsO_2 was present as the result of some process other than fractionation of OsO_4 .

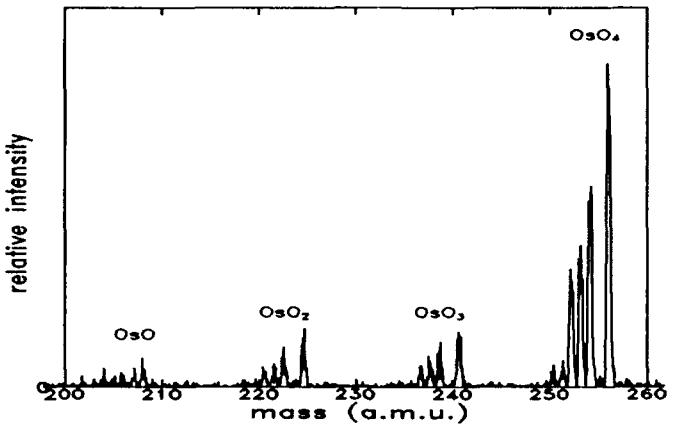

Figure 9. Mass Spectrum of the Osmium Oxides

The data from an appearance potential measurement for OsO_2 is shown in Figure 10. For this measurement the electron energy was scanned over the range 10 to 30 eV for a total of 24 minutes at 1300 K. The total number of ion counts at 30 eV over this time period was only 35. This example demonstrates the advantages of being able to accumulate multiple scans which is made possible through automation of the data acquisition process. Although it is clear that most of the OsO_2 signal appears above 17 eV, indicating that the parent molecule was OsO_4 , the OsO_2 ion signal appearing between 11 and 17 eV must result from the ionization of OsO_2.[13] The osmium monoxide in Figure 9 appeared to form solely as a result of electron impact fractionation of OsO_4.

The signal levels for the oxides decreased with time, indicating that osmium tetroxide was probably an impurity in the osmium powder. The powder is exposed to air each time the vacuum chamber is vented. Upon heating in the Knudsen cell, the trioxide was probably formed via Reaction 18.

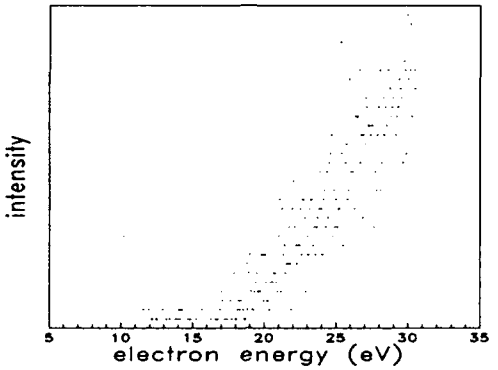

Figure 10. Appearance Potential Measurement for OsO_2

5. CONCLUSIONS

5.1 Analysis of the Instrument and Experimental Method

We have described in this Technical Report the high temperature mass spectrometer and recent improvements made to the system and its data processing capabilities. Replacement of the electron multiplier by a continuous dynode channel multiplier, automation of the data acquisition, and increasing the pumping speed at the ion source of the mass spectrometer has resulted in higher signal-to-noise ratios and in greater sensitivity. A remaining source of uncertainty is the accurate and precise measurement of the temperature of the Knudsen cell. We are currently attempting to measure the temperature using thermocouples placed in different locations on the Knudsen cell; we are also in the process of measuring the temperature using IR optical pyrometry.

5.2 Future Plans

We plan to continue studying the Os-O system by high temperature mass spectrometry using the gas inlet alumina cell. Because the possibility exists that we will not be able to reach a temperature high enough to observe all the gaseous oxides of osmium as well as those of other metals, we are presently preparing an alternative experiment in which the metal sample will be evaporated by laser heating and subsequently reacted with an oxidizing gas. Such an experiment has been described before.[17] It has been found experimentally that molecules with energies of 1 to 10 eV can be produced by varying the power output of the laser.[18] The energy distribution of the beam molecules will be measured by time-of-flight spectroscopy. By measuring the appearance energies of the metal oxides, thermochemical data for these compounds can be derived.[19]

References

1. Peters, P. N., Linton, R. C., and Miller, E. R., (1983) Results of Apparent Atomic Oxygen Reactions on Ag, C, and Os Exposed During the Shuttle STS-4 Orbits, *Geophys. Res. Lett.*, **10**: 569.

2. Peters, P. N., Gregory, J. C., and Swann, J. T. (1986) Effects on Optical Systems from Interactions with Oxygen Atoms in Low Earth Orbits, *Appl. Opt.*, **25**: 1290.

3. Gull, T. R., Herzig, H., Osantowski, J. F., and Toft, A. R. (1985) Low Earth Orbit Environmental Effects on Osmium and Related Optical Thin-Film Coatings, *Appl. Opt.*, **24**: 2660.

4. Murad, E. (1989) Spacecraft Interactions as Influenced by Thermochemical Considerations, *J. Spacecraft*, **26**: 145.

5. For an extensive review see: Drowart, J., and Goldfinger, P. (1967) Investigation of Inorganic Systems at High Temperature by Mass Spectrometry, *Angew. Chem.*, **6**: 581.

6. Bromberg, J. P. (1985) *Physical Chemistry*, Allyn and Bacon, Boston; P. 486.

7. See for example: Skoog, A. D., and West, W. M., (1980) *Principles of Instrumental Analysis*, Saunders College, Philadelphia; p. 481.

8. Gardner, J. A., Dressler, R. A., Salter, R. H., and Murad, E. (1989)*Laboratory Study of Ion-Neutral Collisions at Suprathermal Energies*, GL-TR-89-0345. ADA222117.

9. Inghram, M G., and Drowart, Jean, (1960) Mass Spectrmetry Applied to High Temperature Chemistry, in *Proceedings of an International Symposium on High Temperature Technology*, McGraw-Hill Book Company, Inc., New York; p. 219.

10. Honig, R. E. (1967) Vapor Pressure Data for the Elements, in *The Characterization of High Temperature Vapors*, edited by J. L. Margrave, John Wiley and Sons, New York; p. 475.

11. Atkins, P. W. (1986) *Physical Chemistry, Third Edition*, W. H. Freeman and Company, New York; p. 655.

12. Otvos, J. W., and Stevenson, D. P. (1956) Cross-sections of Molecules for Ionization by Electrons, *J. Am. Chem. Soc.*, **78**: 546.

13. Burrous, C. N., Lieber, A. J., and Zaviantseff, V T. (1967) Detection Efficiency of a Continuous Channel Electron Multiplier for Positive Ions, *Rev. Scient. Intrum.*, **38**: 1477.

14. Hultgren, R., Desai, P. D., Hawkins, D. T., Gleiser, M., Kelley, K. K., and Wagman, D. D. (1973) *Selected Values of the Thermodynamic Properties of the Elements*, American Society for Metals, Metals Park, Ohio; p. 21.

15. Grimley, R. T., Burns, R. P., and Inghram, M. G. (1960) Mass-Spectrometric Study of the Osmium-Oxygen System, *J. Chem. Phys.*, **33**: 308.

16. Dillard, J. G., and Kiser, R. W. (1965) Ionization and Dissociation of Ruthenium and Osmium Tetroxides, *J. Phys. Chem.*, **69**: 3893.

17. Wicke, Brian G. (1979) Laser-vaporization Source for Chemical Kinetics, *Laser Focus*; p. 70.

18. Utterback, N.G., Tang, S.P., and Friichtenicht J.F. (1976) Atomic and Ionic Beam Source Utilizing Laser Blow Off, *The Physics of Fluids*; p. 900.

19. Wicke, Brian G., (1983) Dynamics of the chemiluminescent oxidation of zinc atoms by nitrous oxide, *J. Chem. Phys.*, **78**: 6036.